ICP-1153

Distributed Under Category:
UC-66d
GE: Utilization Technology

Liquid-Fluidized-Bed Heat Exchanger Design Parameters

by

C. A. Allen
E. S. Grimmett

Allied Chemical Corporation
Idaho Chemical Programs - Operations Office

Date Published - April 1978

Prepared for the
Department of Energy
Idaho Operations Office
Under Contract I-(322)-1570

DISCLAIMER

Abstract

Liquid-fluidized-bed heat exchangers prevent scale accumulation on heat transfer surfaces and reduce the required heat transfer surface when scaling fluids such as geothermal water are used as the primary or working fluid. This report describes liquid-fluidized-bed heat exchangers, principles of operation and design parameters. Horizontal and vertical assemblies are discussed, including problems encountered with both designs. Bed-side heat transfer coefficients are given for limited cases, and a correlation is provided for calculating heat transfer coefficients for horizontal assemblies. A design example for a 60 kW(e) (60 $kW_{(electric)}$ preheater is included.

Summary

Liquid-fluidized-bed heat exchangers for geothermal applications are being developed by Allied Chemical Corporation at the Idaho National Engineering Laboratory (INEL) under contract to the Department of Energy (DOE). In a spin-off project from the gas fluidized-bed technology developed at the Idaho Chemical Processing Plant for solidification of radioactive waste, it was found that liquid-fluidized-beds prevented fouling of heat exchanger tubes in an $Al(NO_3)_3$ crystallizer. From this work it was proposed that liquid-fluidized-bed heat exchangers be developed to prevent scale formation in geothermal heat exchangers.

Liquid-fluidized-bed heat exchangers consist of tube-and-shell exchangers with the fouling fluid (geothermal water) passing through the shell side. The water passes up through a bed of particles, such as sand, which surrounds the tube bundle. Between the incipient fluidization velocity and terminal velocity, the bed expands uniformly. The fluidized particles scrub the tube surfaces, keeping them free of scale and increasing heat transfer rates.

Horizontal and vertical tube bundle assemblies have been tested. Vertical assemblies have more uniform fluidization, but usually require large pitch-to-tube diameter ratios. Horizontal assemblies present a larger cross sectional area, and can pass a larger flow with tighter tube packing. Because of the cross-flow nature of horizontal vessels and the constantly changing cross section up the vessel, flow velocity is non-uniform.

Fluidized-beds operate isothermally, so preheaters must be designed with several stages to approach counter-current efficiency. Each stage is a separate heat exchanger, but multiple stages can be put into a single vessel.

Bed-to-tube heat transfer correlations were developed for horizontal heat exchangers. These were developed from data accumulated in tests at the Raft River Geothermal Project supported by DOE. The correlations are given in equations (a) and (b).

$$Nu = (1.82 \pm .18)\left(\frac{dp}{Dt}\right)^{0.2} Re_t^{0.535}\, Pr^{1/3}\, (\varepsilon^{0.535}\,(1-\varepsilon)^{0.465}) \quad (a)$$

where $.4 < \varepsilon < .76$

$$Nu = (1.82 \pm .18)\left(\frac{dp}{Dt}\right)^{0.2} Re_t^{0.535}\, Pr^{1/3}\, (\varepsilon^{0.465}\,(1-\varepsilon)^{0.535}) \quad (b)$$

where $.76 \leq \varepsilon < 1.0$

Using the design constraints described in the report, a design example is given for a 60 $kW_{(e)}$ six-stage preheater. Impact of the constraints becomes clearer when applied to a real heat exchanger.

CONTENTS

TABLES

FIGURES

I. Liquid-Fluidized-Bed Heat Exchanger Description

1. Introduction

1.1 Description

Liquid-fluidized-bed technology offers the potential for scale control in heat exchangers used for geothermal applications. This characteristic was discovered by Hogg and Grimmett[1] with an aluminum nitrate crystallizer. They operated a small liquid-fluidized-bed crystallizer with cooling coils to remove heat from solution. The continual scrubbing of bed particles on the coils prevented deposition of $Al(NO_3)_3$. This property can be used to advantage where heat exchangers are required in geothermal fluids with high scaling potential.

Fluidized beds consist of a bed of solid particles with a fluid passing upward through them. Figure 1 illustrates the behavior of the system as a function of fluid velocity. When the fluid at low velocity is introduced into the bed at rest, the drag force is less than the gravitational force and the fluid seeks the voids between particles. As velocity increases, the pressure drop increases. With further increase in velocity, a point is reached where the fluid velocity applies sufficient drag force on the particles to support them; the bed expands and the fluid/particle system behaves like a fluid. This is called incipient fluidization. At higher velocities, the bed may have either of two fluidization characteristics. In particulate fluidization, each particle acts independently and the bed expands uniformly over the fluidization range. Aggregative fluidization occurs when packets of particles move together, and bubbles or voids move up through the bed. This action is much more vigorous, and gross recirculation occurs. When the fluid velocity exceeds the particle settling velocity (terminal velocity), particles are entrained in the fluid and elutriated.

Why liquid-fluidized-beds exhibit particulate fluidization and gas-fluidized-beds aggregative fluidization is not clearly understood. Botterill[2] suggests that the fluidization mechanism depends on the ratio of fluid to particle density. As the ratio of densities approaches one, particulate fluidization occurs. When the density of the particles

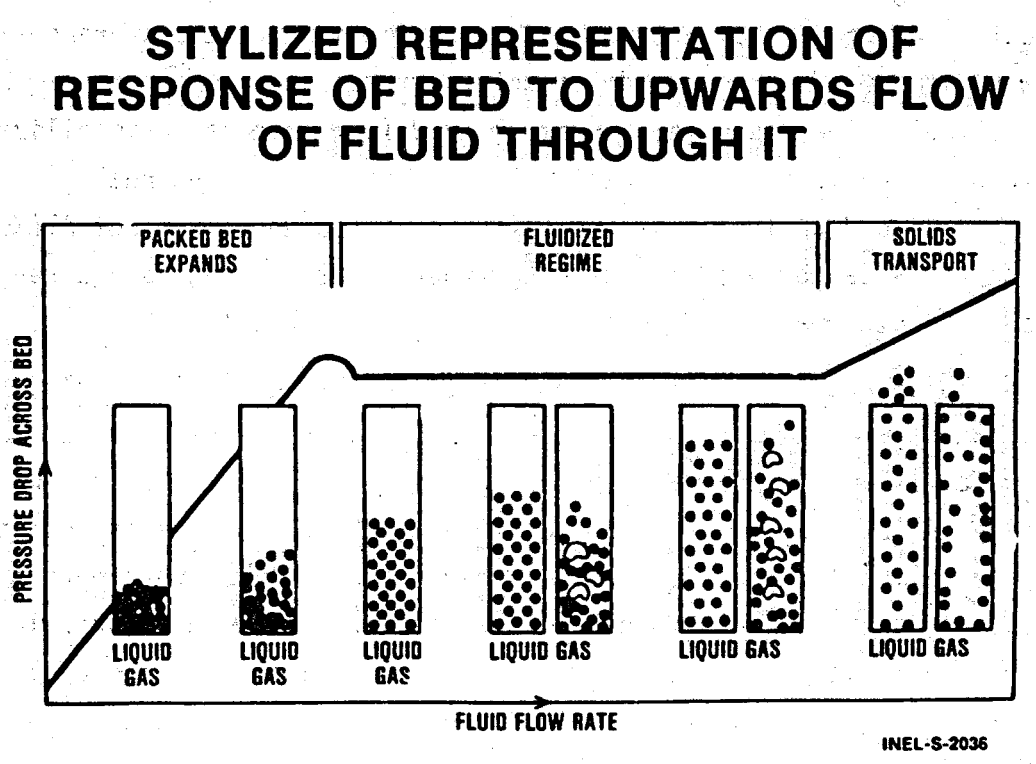

Figure 1. Schematic Representation of Fluidization as Function of Fluid Flow Rate. Fluidizing fluid is either liquid or gas as shown. (After Botterill)[2]

is much greater than the fluid density, aggregative fluidization results. In general, liquid-fluidized-beds exhibit particulate fluidization and gas-fluidized-beds aggregative fluidization. The density relationship was supported by Patel and Simpson,[3] who found aggregative fluidization in beds of lead shot fluidized with water and particulate fluidization with beds of glass beads fluidized with water.

Gas-fluidized-bed technology is well developed and has been used extensively for particle coating, calcination, and drying. However, liquid-fluidized-bed technology remains relatively undeveloped. The largest body of literature is the result of the feasibility study of a liquid-fluidized-bed nuclear reactor. This deals with heat transfer from particles, which contain fuel, to the liquid, which acts as a coolant and moderator. A summary of this work through 1966 is published by A. C. Trupp.[4]

Liquid-fluidized-bed heat exchangers are made by immersing a tube bundle or coil in the bed. In this case, the geothermal fluid is on the shell side of the exchanger and the secondary fluid on the tube side. This reverses the normal design of the geothermal heat exchangers where the geothermal water passes through the tubes to facilitate scale removal. There are two advantages to putting the geothermal fluid on the shell side.

1. Organic secondary fluids transfer heat at a lower rate than water. Putting them through the tubes at high velocity substantially increases the overall heat transfer rate.

2. Geothermal brine is usually at lower pressure than the secondary fluid. This reduces the design requirement on shell thickness and lowers the cost.

Liquid-fluidized-bed heat exchangers consist of the four parts shown in Figure 2.

1. Flow distribution-support system: Geothermal flow through the bed must be uniform. Distribution is accomplished in the plenum by regulating the pressure drop across the distribution-support system or by physically distributing the fluid with a manifold.

2. Fluidized-bed: The bed of particles is contained by the shell, and the height of the bed is regulated by the quantity of bed material, the particle diameter, the particle density, the fluid density, the fluid viscosity, and the fluid velocity. Bed material which has been tested so far consists of silica sand closely screened to the desired size.

3. Disengagement space: Between the top of the bed and the geothermal outlet, a space must be allowed for particles to be disengaged from the fluid and fall back to the bed. Liquid-fluidized-beds normally exhibit a sharp interface at the top of the bed due to their particulate fluidization mechanism. As a result, the disengagement space can be much smaller than that allowed in gas-fluidized-beds.

4. Tube bundle: The secondary fluid flows through the tube bundle, which is immersed in the bed.

The shell of liquid-fluidized-bed heat exchangers can be arranged either vertically as in Figure 2 or horizontally as in Figure 3. In either case, the geothermal fluid flows vertically through the bed on the shell side. The choice of horizontal versus vertical arrangement is based on mass flow rate, heat transfer surface requirements, cost, and physical limits.

The primary characteristic of fluidized-bed heat exchangers which causes design to differ from conventional units is their isothermal nature. This is due to the rapid mixing of the bed particles. Because of this property, liquid-fluidized-bed heat exchangers must be staged to approach counter-current efficiency.

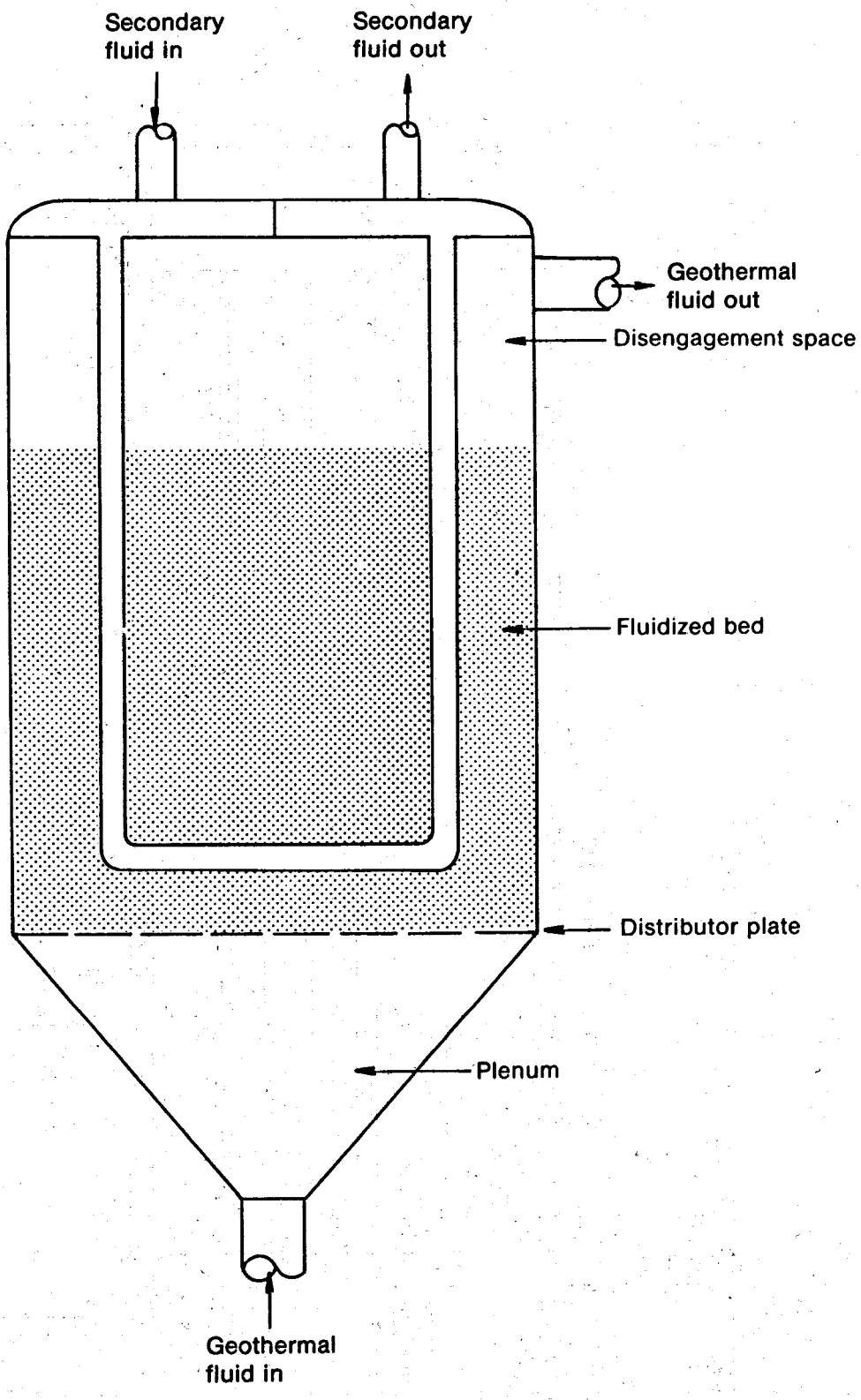

Figure 2. Diagram of a Double-Pass, Vertical, Liquid-Fluidized-Bed Heat Exchanger

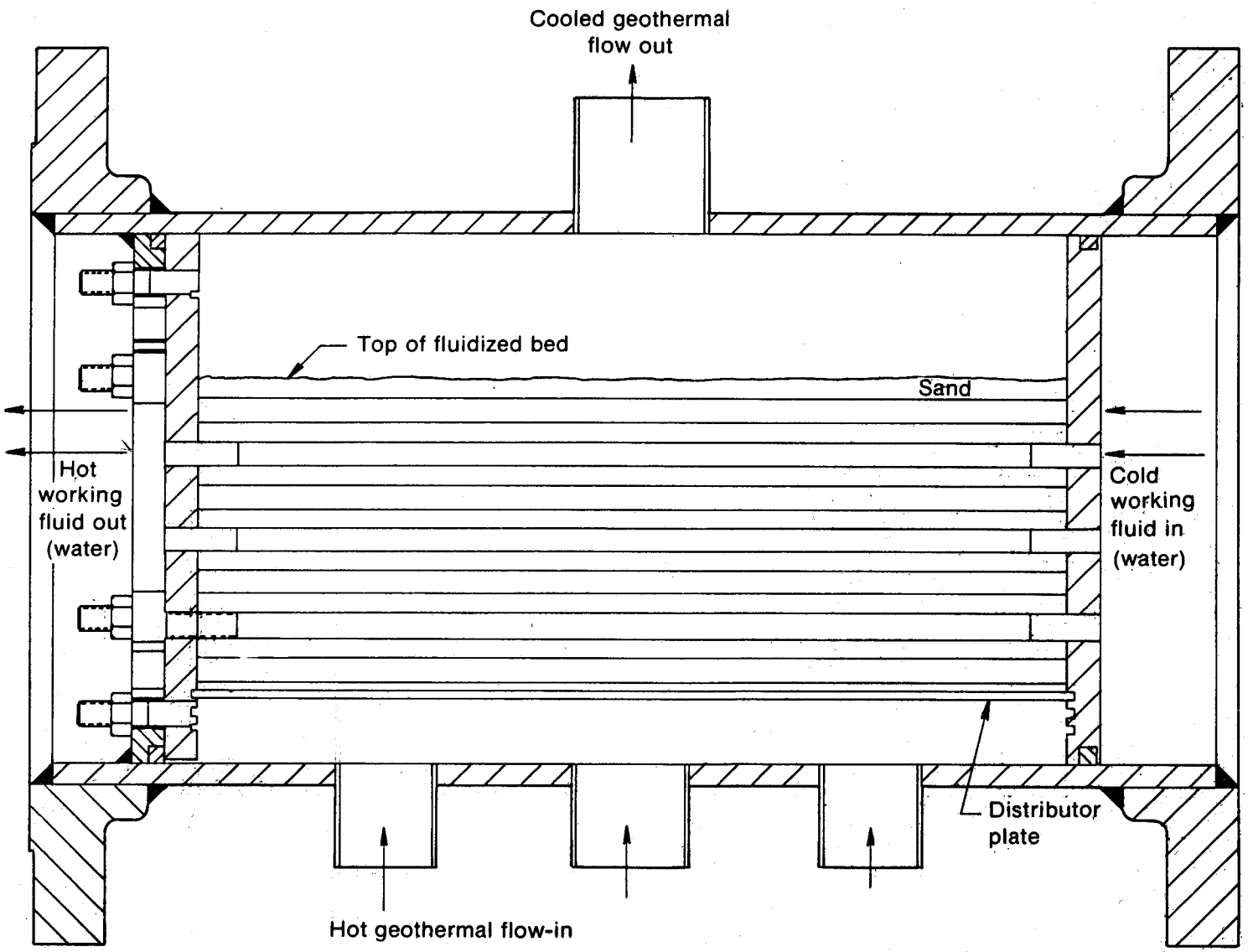

Figure 3. Horizontal Arrangement of a Liquid-Fluidized-Bed Heat Exchanger

1.2 Heat Transfer Mechanism

Typically, the heat transfer coefficients in fluidized beds exceed by at least a factor of 1.5 coefficients with no bed present. The primary cause is believed to be the continual erosion of the thin film barrier surrounding the tubes. This heat transfer increase is related to the frequency of contact between particles and tubes. This in turn is related to the density of particles (porosity), particle size, and particle velocity. Both porosity and particle velocity are related to the fluid velocity, density, and viscosity.

1.3 Potential Advantages

Control of scale in geothermal systems provided the impetus for development of liquid-fluidized-bed heat exchangers. Many hydrothermal systems can only be developed economically by using a binary system. On the other hand, most geothermal water has high scaling potential. This requires that heat exchangers be designed by anticipating a high fouling rate. Such designs are costly because of the high cost of heat transfer surface. This is especially true in geothermal systems where the temperature is low and the ratio of surface area to heat transferred is high. By reducing or eliminating scale deposit on heat exchanger surfaces, the economics of hydrothermal systems will be favorably altered.

Wagner[5] demonstrated with bench-scale equipment and synthetic fluids that a liquid-fluidized-bed prevents deposition of calcite and amorphous silica. Figure 4 shows the heat transfer coefficient in super-saturated fluids with and without a bed. Two mechanisms are postulated for scale control characteristics in a fluidized bed.

1. The bed provides sufficient abrasive action to continually scrub the heat transfer surfaces. This mechanism is supported by experiments at Raft River. After 60 days of operation, the heat transfer surfaces were highly polished. Also, during experiments with silica and $CaCO_3$ super-saturated solutions, neither the particles nor the tube surface received deposit.

2. The surface area of the bed exceeds the heat transfer surface area by about 50 times.[6] The large difference will cause deposits to form on the bed particles rather than the heat transfer surface. This mechanism may be important for very hard deposits such as iron sulfide.

For most waters with scaling potential, the first mechanism may be more important.

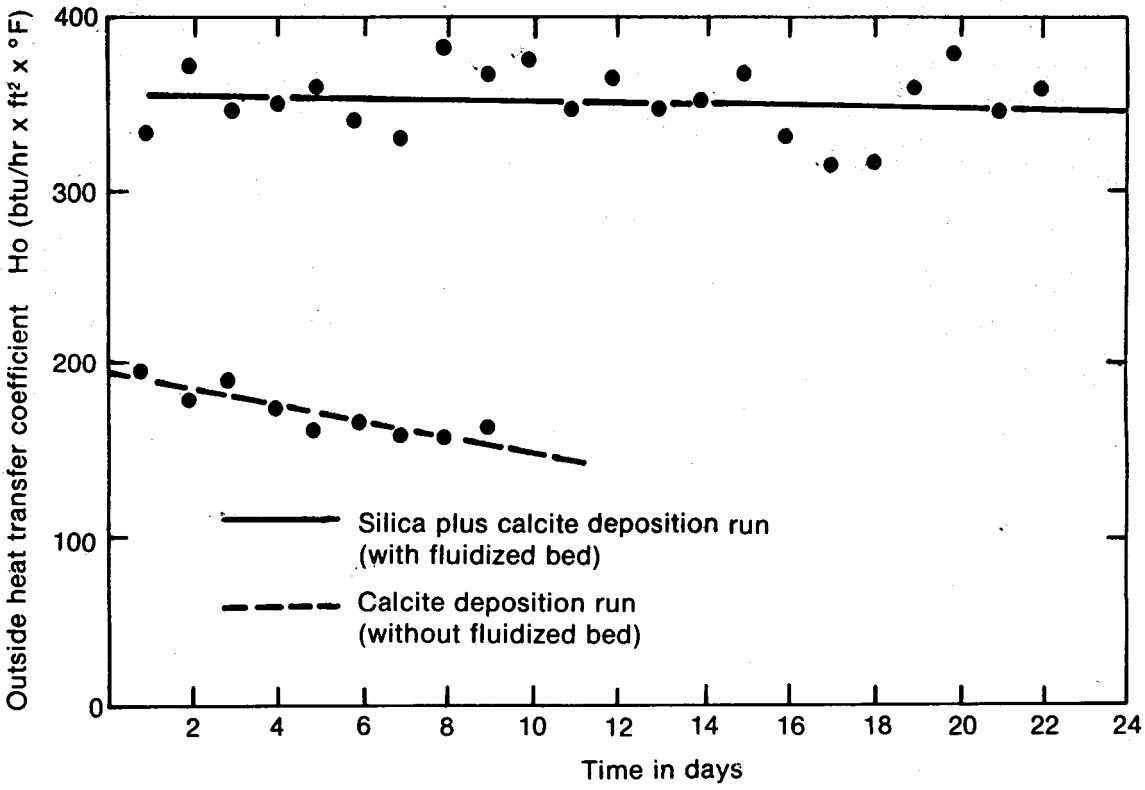

Figure 4. Bed-to-Tube Heat Transfer Coefficients from a Bench-Scale Experiment Using Synthetic Supersaturated Fluids.

1.4 Possible Applications

Liquid-fluidized-bed heat transfer technology is applicable to preheaters and boilers in a binary cycle power plant. Liquid-fluidized-beds might also be used in the condenser. Incentive for application to the condenser stems from reduced heat transfer surface requirements and the potential for using untreated brine for heat rejection. The basic technology is similar for all these applications. The following sections will deal with liquid-fluidized-bed behavior and the unique problems of liquid-fluidized-bed heat exchanger design.

II. Fundamentals of Liquid-Fluidized-Bed Behavior

1. Definitions of Liquid-Fluidized-Bed Terms

1.1 Fluidization Velocity

For an ideal system, the minimum fluidizing velocity, where incipient fluidization occurs, is defined as the velocity at which the bed changes from a fixed to a fluidized state. In practice, however, incipient fluidization does not occur uniformly due to fluctuation of velocity, cross-flow around tubes, and vessel configuration. A theoretical calculation of minimum fluidizing velocity inside a shell-and-tube heat exchanger is difficult, but approximation of its velocity can be done experimentally by using the graph of a frictional pressure drop against velocity (Figure 5).

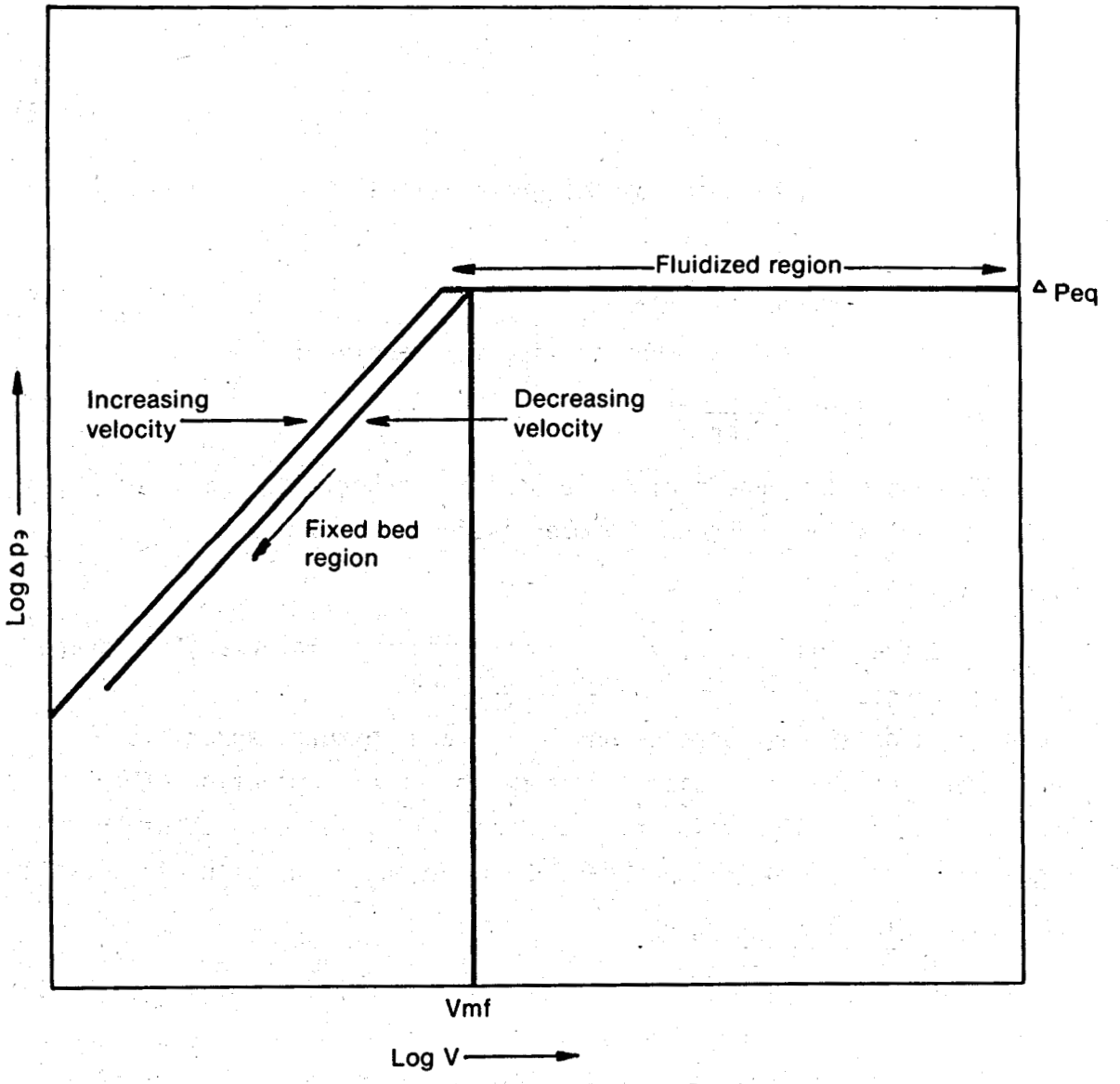

Figure 5. Ideal Pressure Drop-Velocity Curve

1.2 Superficial Velocity

Superficial velocity is the vertical component of fluid velocity through the shell, assuming the shell contains only fluid.

$$v_o = \frac{1}{\rho_f A_c} \frac{dM}{dt} \tag{1}$$

1.3 Terminal Velocity

Terminal velocity is defined as a velocity of a solid particle falling freely from rest in a stationary fluid under the action of gravity. The terminal velocity (v_t) for a sand particle can be derived as follows:

The drag force around a sphere of diameter (dp) is defined by:

$$F_k = \left(\frac{\pi dp^2}{4}\right) \left(\tfrac{1}{2} \rho_f v_t^2\right) D_c \tag{2}$$

This force is balanced by the gravitational force minus the bouyancy force on the sphere.

$$F_k = 1/6 \ \pi dp^3 g_c(\rho_s - \rho_f) \tag{3}$$

Equating (2) and (3) then solving for v_t gives:

$$v_t^2 = \frac{4 \ g_c dp \ (\rho_s - \rho_f)}{3 \ D_c \qquad \rho_f} \tag{4}$$

Where the drag coefficient (D_c) with a sphericity factor of 0.806 (sand) and high Reynolds number is found to be about 1.6.

1.4 Void Fraction

Void fraction (porosity = ε) is a measure of interparticle space and is expressed as: $\varepsilon = 1 - \frac{\text{Volume of Sand}}{\text{Total Volume}}$

Void fraction at rest depends on the surface texture, sphericity, uniformity of the grain size, and cementation or compaction of the sand. Expressed as a void fraction, the normal value is about 0.42% after sedimentation. Void fraction depends on velocity in a fluidized system.

1.5 Particle Size and Shape

The particle size as used here is a mean particle diameter (MPD) with standard deviation of about $\pm$30%. Particle shape is expressed by the sphericity factor, which is defined as the ratio of surface area of

a sphere having the same volume as the particle to surface area of the particle. For sand, the sphericity is found to be 0.806.

2. Void Fraction Versus Reynold Number Relationships for Bed Expansion

Liquid-fluidized-beds exhibit the characteristic of a streamline liquid. The bed expands smoothly as velocity is increased from the incipient fluidizing velocity to terminal velocity, assuming uniform particulate fluidization. As the liquid velocity increases, the height of the bed increases, and particle concentration decreases until eventually particles become entrained in the liquid and escape from the bed. The free settling velocity of a particle is not directly applicable to suspensions of large numbers of particles, where neighboring particles interfere with each other. Hence, the effect of the settling velocity is reduced. This reduction ratio may be expressed in the form of the porosity (ε) and superficial velocity (v_o).

$$v_o = v_t \varepsilon^m \tag{5}$$

Lewis, (et.al.)[7] proposed the empirical relation, equation (6), for uniform size catalyst particles fluidized in liquids.

$$v_o = 0.72\, v_t \varepsilon^{2.33} \text{ for } R_e = \frac{\rho_f v_o d_p}{\mu_f} > 500 \tag{6}$$

Richardson and Zaki[8] conducted extensive experiments and established empirical correlations for the exponent 'm' as a function of R_e and d_p/D_t.

$$v_o = v_i \varepsilon^m \tag{7}$$

$$\text{where } \log v_i = \log v_t - d_p/D_t \tag{8}$$

$$\begin{aligned} m &= 4.45 + 18(d_p/D_t)\, R_e^{-0.1} && \text{for } 1 < R_e < 200 \\ m &= 4.45\, R_e^{-0.1} && \text{for } 200 < R_e < 500 \\ m &= 2.39 && \text{for } R_e > 500 \end{aligned} \tag{9}$$

However, Richardson in a more recent report shows this equation is unreliable under conditions where uniform fluidization is not obtained. In heat exchangers, the tube bundle makes uniform fluidization very difficult to achieve. This leads to increased d_p/D_t dependence in equation (5). Our proposed equation is:

$$v_o = v_t \varepsilon^m \qquad (10)$$

where $m = 8.85/\log(d_p)$, d_p is in microns and $1 < R_{ep} < 200$

This relation was extrapolated from Wilhelm and Kwauk's[9] work and our own data on sand fluidized with water, as shown in Figure 6.

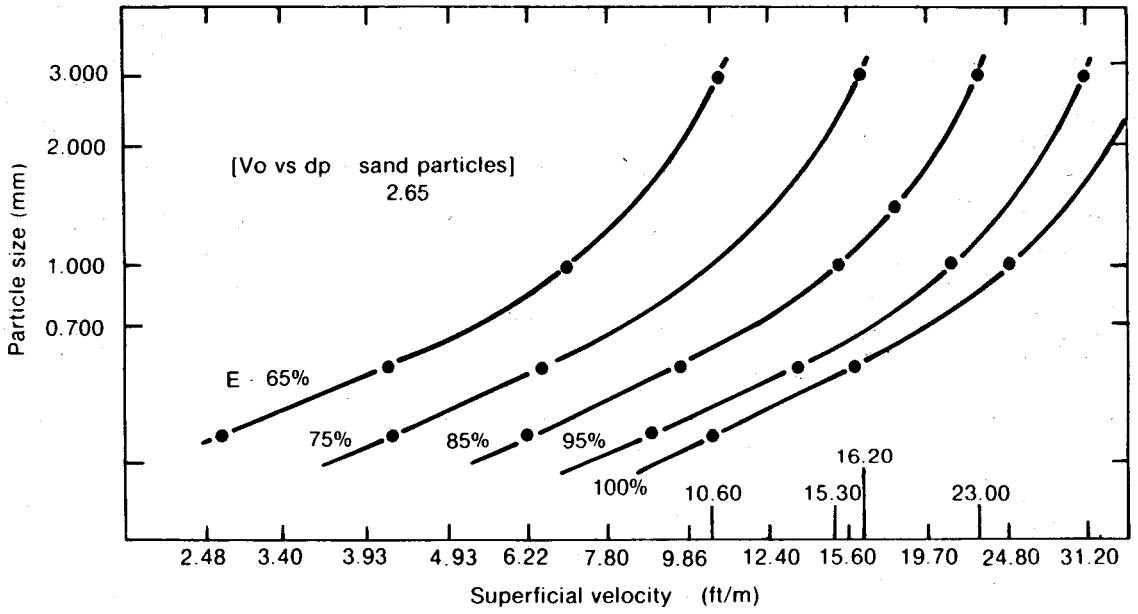

Figure 6. Variation of Porosity with Superficial Velocity for Various Particle Sizes (ft/min = 5.08×10^{-3} m/sec) T=135°C

3. Dimensional Analysis

A number of correlations have been proposed for calculating surface heat transfer coefficients for both vertical tubes and horizontal tubes in fluidized beds. In general, the results of these experiments have been correlated empirically on the basis of a limiting film and bed resistance at the heat transfer surface.

The most adequate papers on the studies of heat transfer in liquid fluidized-bed are those by: Hamilton,[10] Brea (et.al),[11] Richardson (et.al),[12] Ruckensten and Toereanu,[13] Chu (et.al.),[14] and Wasmund and Smith.[15]

All workers, except Ruckenstein and Wasmund, agree that the dimensional groups are arranged in the following general form:

$$Nu = a\, Re_t^b\, Pr^e\, \varepsilon^d\, (1-\varepsilon)^e \left(\frac{d_p}{D_t}\right)^f \qquad (11)$$

The constant and exponents (a, b, c, d, e, f) are found experimentally in the following way: Hamilton and Brea correlate their data by Chu's Colburn J-factors where Richardson uses Jagnnadjaraju's[16] Colburn J-factors. Our data fits Chu's J-factor. The J-factor is defined as:

$$J = \frac{Nu}{Re_o \ Pr^{1/3}} \tag{12}$$

and Chu;s J-factor is

$$J = C \left(\frac{Re_o}{1-\varepsilon}\right)^{n-1} \tag{13}$$

where C is a constant.

Superficial velocity (v_o) and terminal velocity (v_t) in the intermediate to turbulent flow region are related by:

$$Re_t = Re_o \ (\varepsilon)^m \tag{14}$$

$$\text{where } m = \frac{8.85}{\log d_p} \tag{15}$$

Substitution of (14) into (12):

$$Nu = C \ Pr^{1/3} \ Re_t^{n-1} \ \Phi \ (\varepsilon) \tag{16}$$

where $\Phi \ (\varepsilon) = (\varepsilon^{m(n-1)} \cdot (1-\varepsilon)^{1-n})$ and when d_p = 1 mm MPD sand,

$$m = \frac{8.85}{\log d_p} = 2.95 \tag{17}$$

From Figure 7, the slope (n-1) has an average value of -0.465; and the constants b and e were 0.535 and 0.465, respectively. The constant e has a value of 1/3 defined by the J-factor. The constant d is 0.535 after some algebraic calculation. The constants a and f were determined to be 1.823 $\pm$ 10% and 0.2, respectively, by trial-and-error method to fit our experimental data (see Figure 8). Substitution of these constants into equation (11) gives:

$$Nu = (1.823 \pm .182) \left(\frac{d_p}{D_t}\right)^{0.2} Re_t^{0.535} \ Pr^{1/3} \ (\varepsilon^{0.535m} \ (1-\varepsilon)^{0.465} \tag{18}$$

This correlation is valid when porosity is between 0.4 and 0.76. When porosity is above 0.76, a correction has been made to adapt the equation to the observed maximum when the outside heat transfer coefficient is plotted against velocity or porosity.

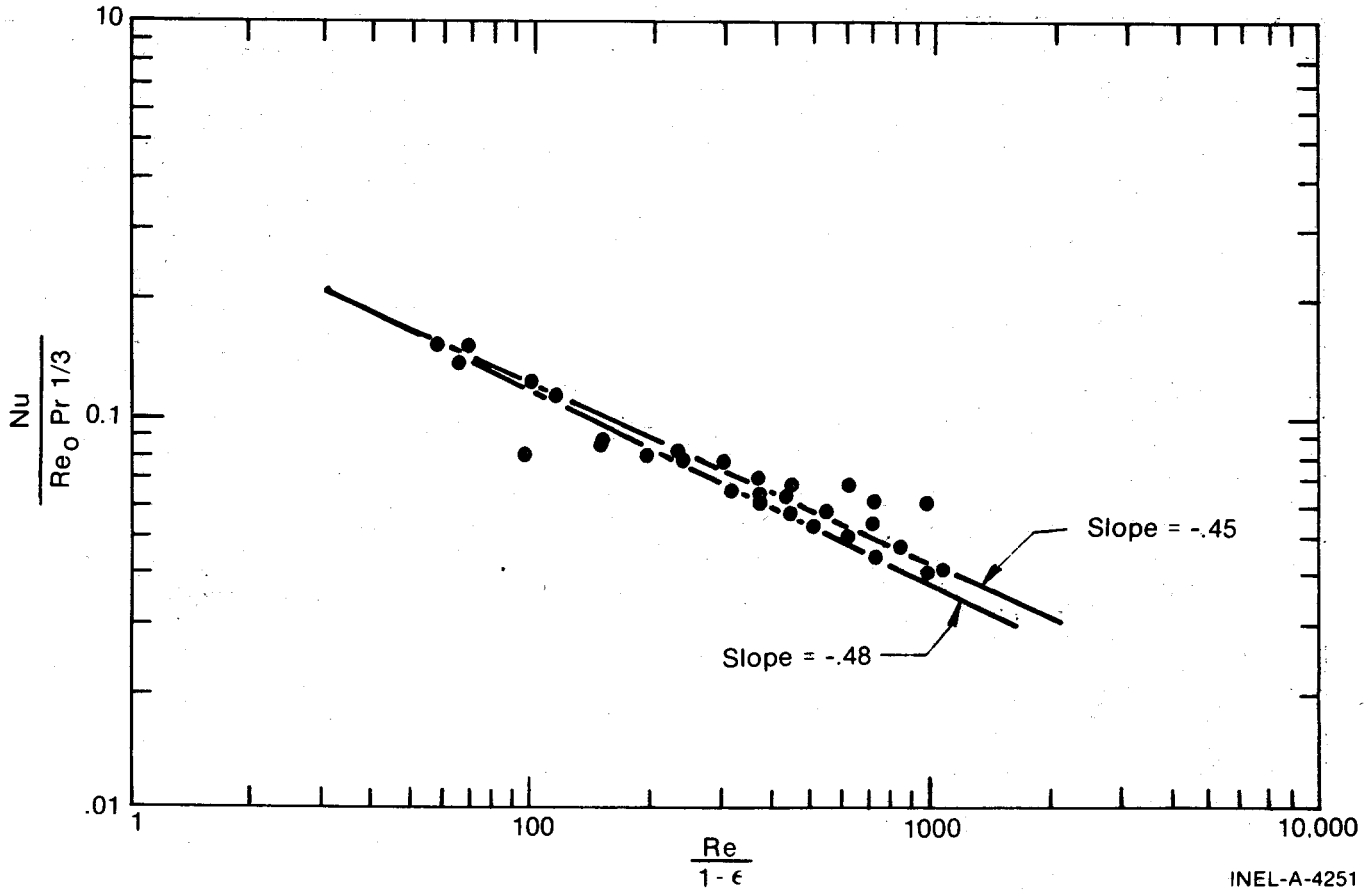

Figure 7. Determination of the Constant n-1 from Equation (16)

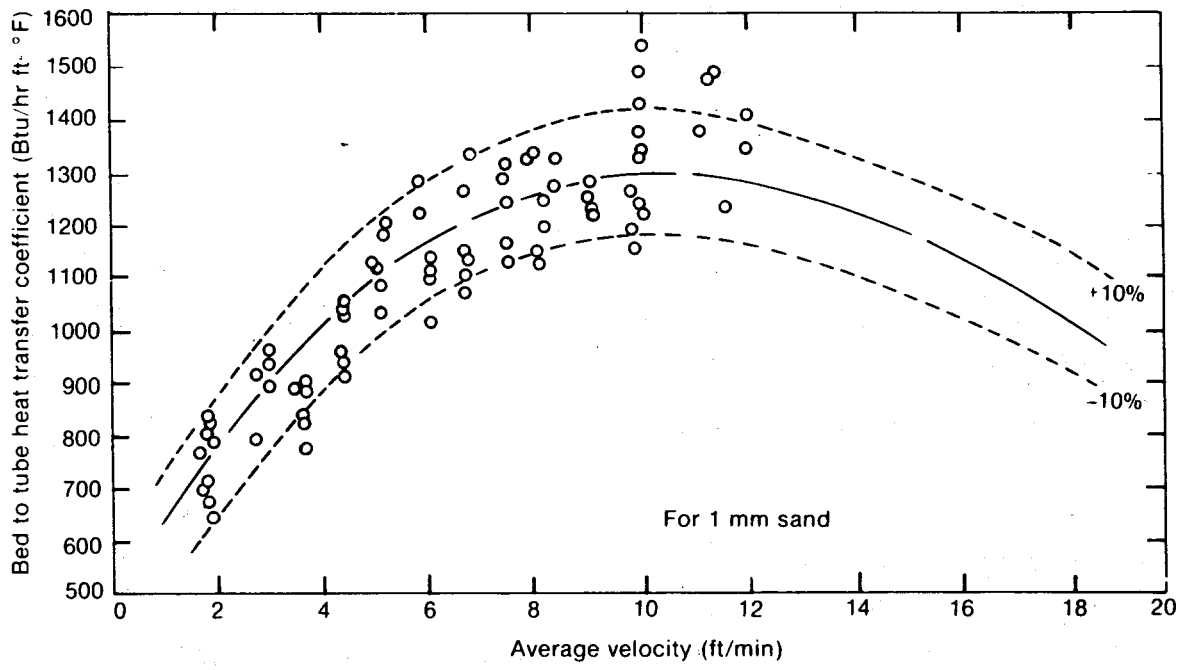

Figure 8. Experimental Heat Transfer Values compared to the Calculated Values from Equation (18)

$$Nu = (1.823 \pm .182)\left(\frac{d_p}{D_t}\right)^{0.2} Re_t^{0.535}\, Pr^{1/3}\, (\varepsilon^{0.465m}\,(1-\varepsilon)^{0.535} \quad (19)$$

Table I compares the values of the constants determined by our work with those obtained by other investigators. The correlation is similar to Hamilton's, but a comparison of Nu numbers shows an average deviation of -40% for Hamilton and Brea. The Richardson equation gives a 60% higher value, yields different curve shapes, and the maximum occurs near a porosity of 0.65.[17]

Table I

Comparison of Coefficients for Equation (11) Using Different Experimental Data and Methods of Correlation

	INEL W/A Bundle of Tubes	INEL W/Single Coiled Tubes	Hamilton & Brea	Hamilton's Form of Wasmumd & Smith	Richardson et al
a	1.823	1.48	0.943	3.38	0.67
b	0.535	0.535	0.55	0.565	0.62
c	1/3	1/3	0.52	1/3	1/3
d	0.535m	0.535m	0.55m	0.656m	0.62m-1
e	0.465	0.465	0.45	0.435	0.38
f	0.2	0.2	0.15	0.57	-0-

III. Fluidized-Bed Geometry

1. Staged Flow

Because of rapid mixing in a dense-phase liquid-fluidized-bed, the shell-side temperature distribution approaches isothermal. Changes in circulation patterns do cause temperature variations within the bed, but the isothermal approximation adequately describes the heat exchanger behavior.

Table II illustrates temperature variations normally seen in a liquid-fluidized-bed over the flow range from below incipient fluidization to about two-thirds of the way through the fluidization range. Thermocouples were located at the bottom, middle, and top of the bed. The data were collected in a small-scale horizontal heat exchanger operating on geothermal water with cooled treated water as the secondary fluid.

Table II

Temperature Variation in a Fluidized Bed

Average Verlocity (ft/min)	Temperature (°F)					
	In	Bottom	Middle	Top	Out	
2.35	274	258	238	224	217.4	below incipient fluidization
4.52	275	268	262	258	239.3	quiescent state
6.36	274	270	254	261	244.7	active bed
8.40	274	273	256	265	252.9	" "
10.1	274	270	261	263	253.7	" "
12.4	273	271	262	262	257.4	" "
15.0	275	272	267	266	259.9	" "

As seen in Table II, below the point of fluidization, or when the bed is in a quiescent state, the temperature profile is normal, i.e., the bottom temperature is highest and the top the lowest. Between velocities of 6 feet per minute and 12 feet per minute, the top and middle bed temperatures were inverted. This is due to circulation patterns established in the bed. Above 12 feet per minute, the top and middle temperatures of the bed are isothermal due to vigorous mixing. The bottom temperature remains high indicating less mixing.

Isothermal behavior impacts heat exchanger design by requiring a unit to be staged to approach counter-current efficiency. In essence, each stage is a separate exchanger, although it is possible to place more than one stage in a single vessel. The stages are arranged such that the geothermal brine entry stage is the exit stage of the secondary fluid. Examples of possible arrangements are shown in Figures 9 and 10. Figure 9 illustrates the arrangement of three horizontal stages contained in a single shell. With this arrangement, the geothermal brine is directed between stages by baffles. Figure 9 shows vertical stages stacked in a tower.

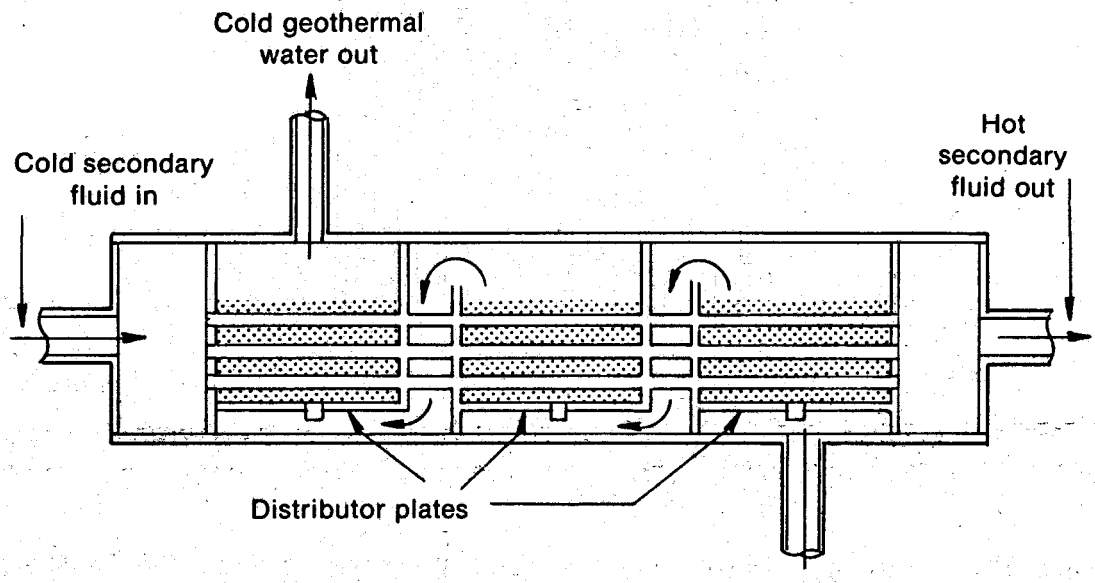

Figure 9. Possible Arrangement of Stages in a Horizontal Liquid-Fluidized-Bed Heat Exchanger

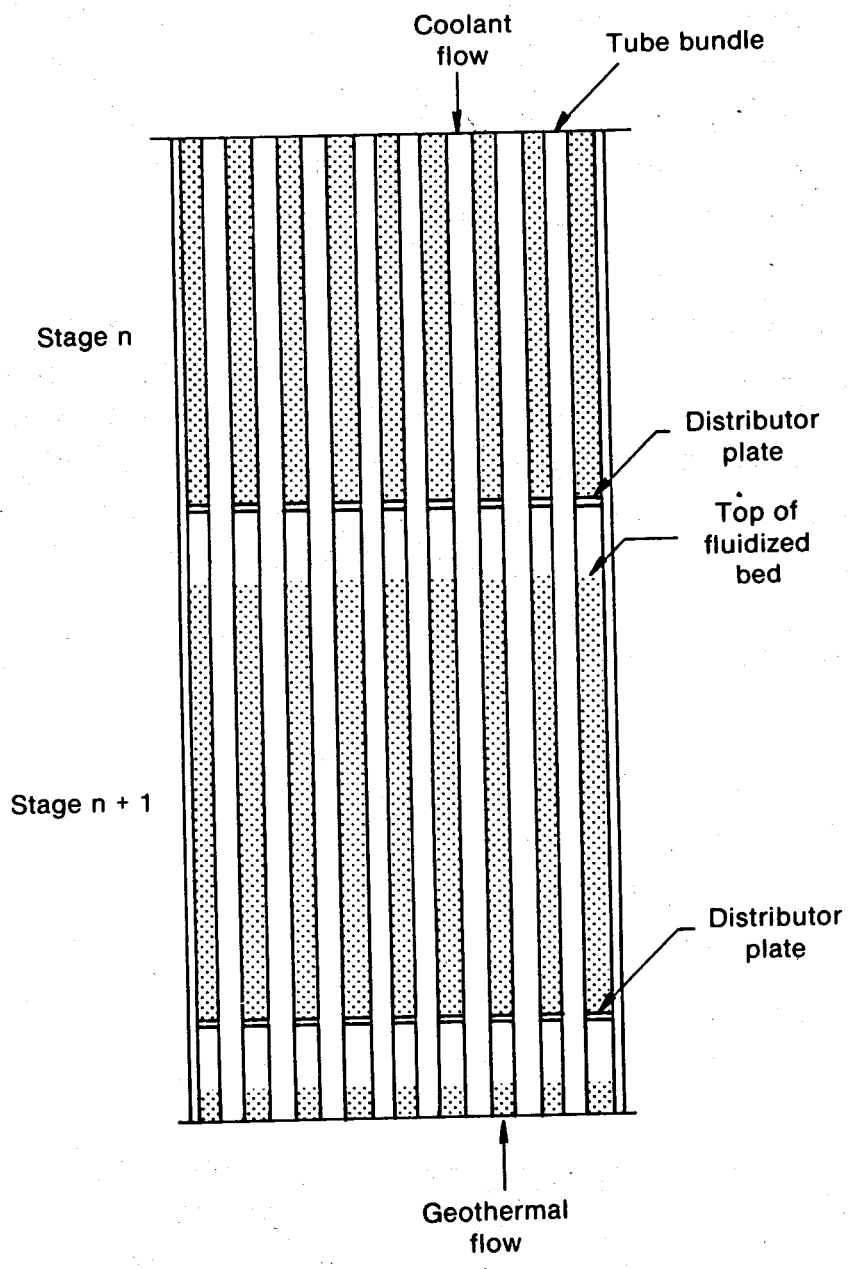

Figure 10. Vertical Liquid-Fluidized-Bed Arrangement with the Geothermal Fluid Routed Internally Between Stages

Cost, efficiency, and brine velocity must be considered when determining the number of stages for a heat exchanger. By increasing the number of stages, the efficiency increases, requiring less total heat transfer surface. Efficiency approaches true counter-current efficiency asymptotically. However, increasing the number of stages increases the cost linearly. An optimum is reached when adding a stage balances the cost saving in tube surface with the increased cost of the extra stage.

Each stage is limited in cross-sectional area by the velocity requirement. The brine velocity through the shell-side is limited by the window bounded by incipient fluidization and terminal velocity. However, to operate near the maximum heat transfer coefficient, the limitation is more severe. Figure 11 shows experimental bed-to-tube heat transfer coefficients as a function of velocity and particle size. For each particle size, there exists a velocity which produces a maximum heat transfer coefficient. This occurs near the porosity of 0.7 to 0.75.

Figure 6 relates particle size to velocity and porosity. The cross-sectional area of a stage must be arranged such that the fluid velocity allows particles to be in the porosity range of 0.7 to 0.75. Not only velocity, but particle size is an important design parameter.

2. Flow Distribution Systems

Fluidization depends on fluid velocity, and uniform fluidization depends on a uniform cross-sectional velocity profile. Uniform velocity is provided by distributing the flow beneath the tube bundle and bed. Fluid enters the bottom of the shell via a pipe or manifold. The flow is partially dispersed in the plenum. In this segment of the shell the flow cross section is increased from the cross-sectional area of the delivery system to the cross section of the support-distribution plate.

The support-distribution plate supports the bed and is the final part of the flow distribution system. The simplest system consists of a single perforated plate with the perforation diameter smaller than the particle diameter. This system is limited to non-scaling brines since small perforations are easily plugged.

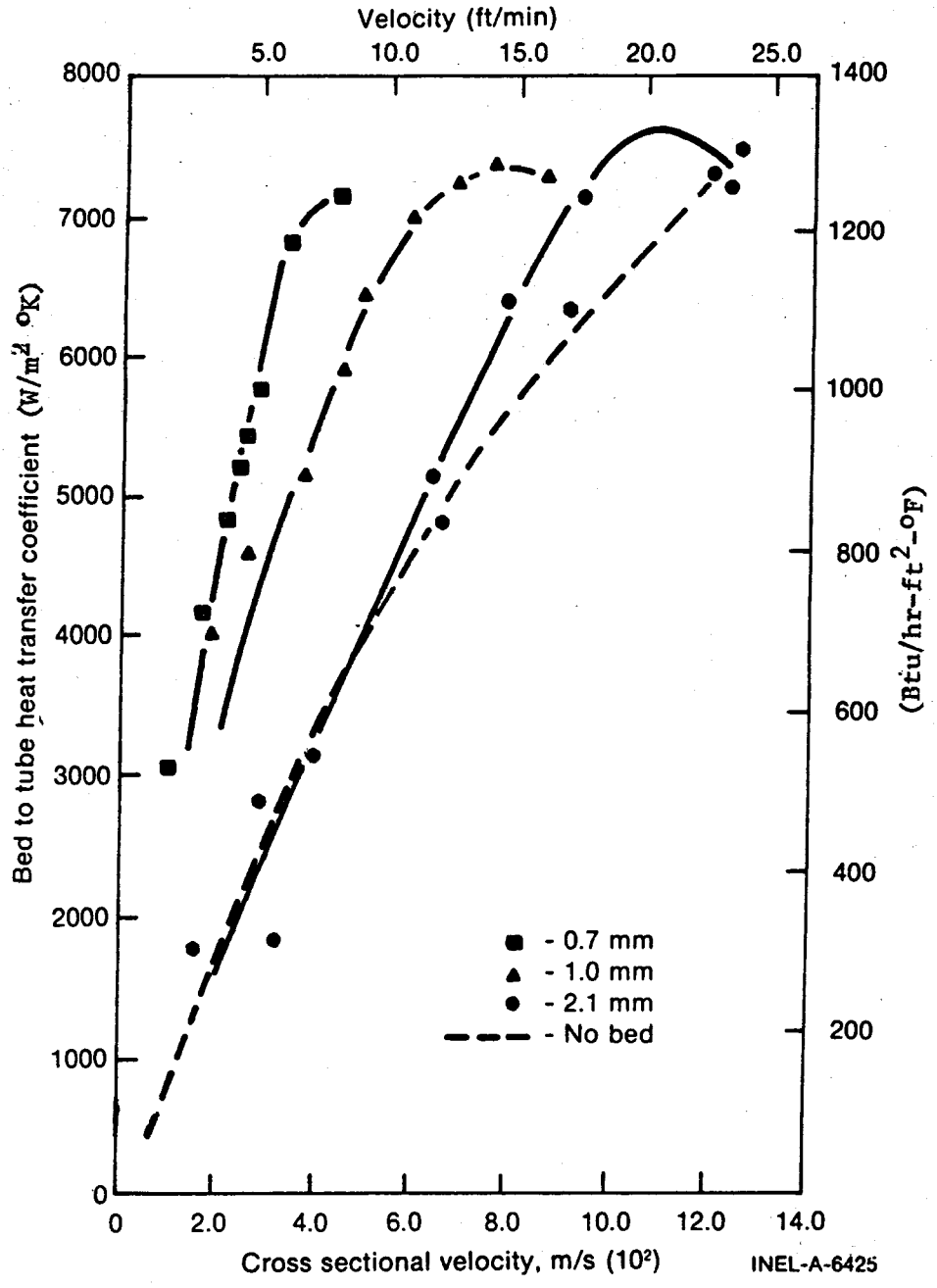

Figure 11. Bed-to-Tube Heat Transfer Coefficients for a 2-cm Horizontal Vessel as a Function of Cross-Sectional Velocity at a Geothermal Inlet Temperature of 135°C

A second type of distributor has large perforations in the plate, with back-flow of the sand prevented by bubble caps over each hole. This is shown in Figure 12. The overlap of the cap and its distance above the plate is governed by the angle of repose of the bed material at rest. This system is not affected by some scaling on the bottom of the plate. It also allows large particles to pass through the distributor without plugging it. The primary disadvantage is the cost of fabrication. This is similar to the distributor plate used in the fluidized-bed calciner for solidifying radioactive waste at the Idaho Chemical Processing Plant. This system was also used in a scale control experiment at East Mesa in Imperial Valley, California.

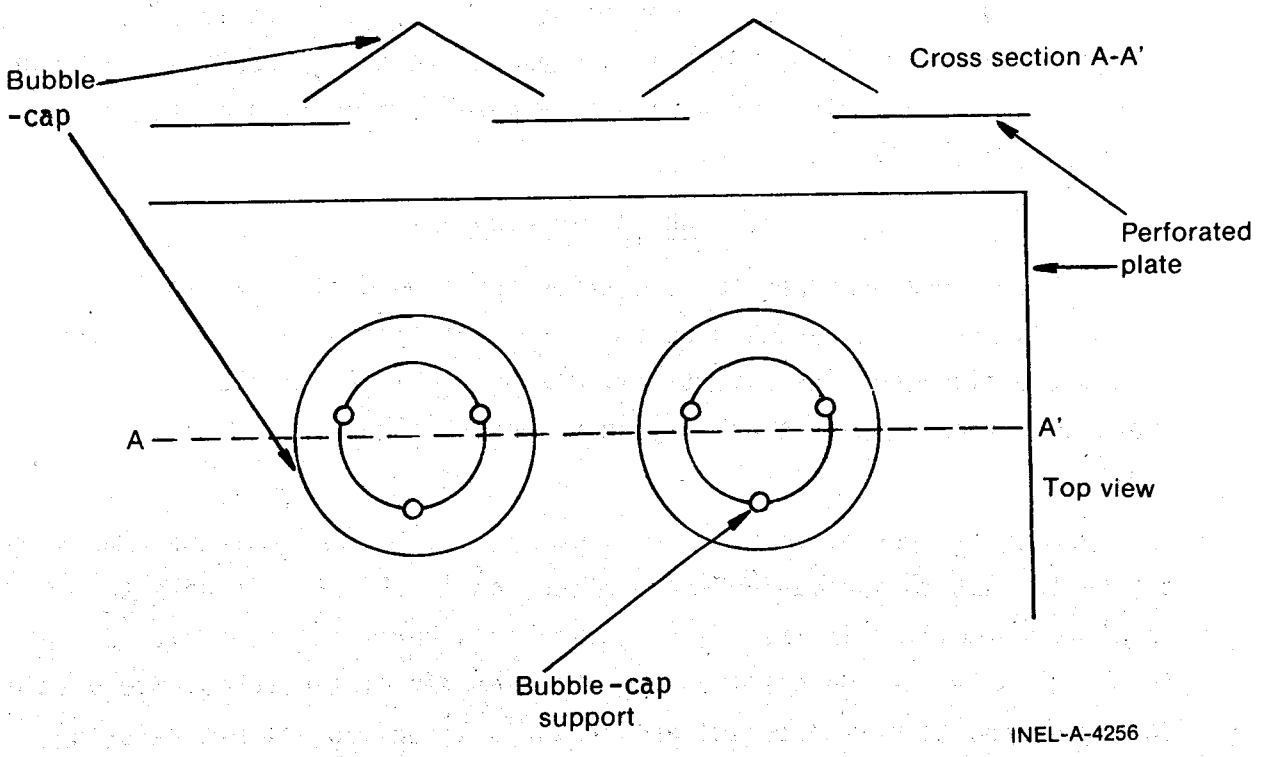

Figure 12. Section of a Bubble-Cap Distributor Plate

A combination distributor simulates natural liquid fluidized beds found in quicksand. In this system, the plenum is filled with pebbles or steel balls which are relatively stationary, but distribute the flow. This system is known as a pebble bed and has been used successfully in bench-scale experiments. At rest the bed is supported by the pebble bed. During flow conditions there is enough agitation in the pebble bed to prevent scale formation in the distributor. The major disadvantage of this system is added weight, which increases support costs.

Gas fluidized beds maintain the most uniform fluidization when the pressure drop across the distributor plate is 40% of the pressure drop across the bed. A similar rule of thumb is not yet available for liquid-fluidized-beds, but work is proceeding in this direction. Pressure drop across the distributor represents a parasitic pumping cost, and needs to be minimized.

3. Tube Arrangement

The two designs under consideration for liquid-fluidized-bed heat exchangers present separate problems involving flow around tubes. The vertical design contains a vertical tube bundle with parallel flow characteristics. In this case fluid velocity is constant on the shell-side.

Horizontal vessel design presents more complex problems because of the cross-flow nature and variable cross section.[18] Figure 13 shows the relative velocities in the cross section of a horizontal vessel. D_S is the diameter of the shell and D_O the diameter of the tubes. Velocities in various parts of the vessel are shown as a function of pitch-to-tube diameter ratio. Variable velocity creates the situation where the velocity at the bottom of the exchanger could exceed terminal velocity while the top of the bed appears normal. When designing horizontal exchangers, it is imperative to calculate the maximum velocity as well as the cross-sectional velocity.

Conventional tube-and-shell heat exchangers have a pitch-to-tube diameter ratio of about 1.25. This is undesirable in liquid-fluidized-bed heat exchangers because the particle size becomes a significant

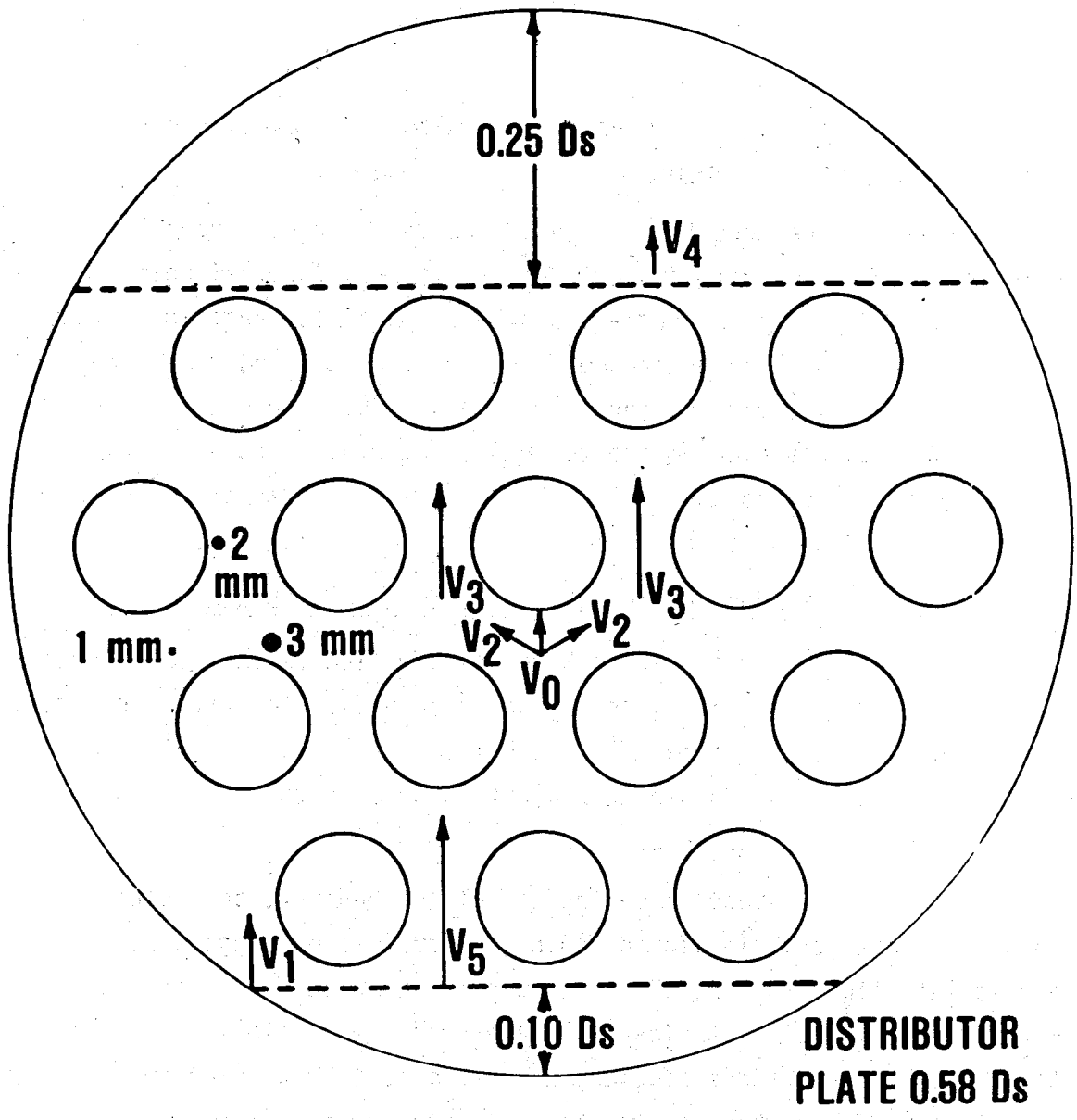

V_0 = SUPERFICIAL VELOCITY (VELOCITY THROUGH THE CENTER WITH NO TUBES PRESENT

p/Do	V_1	V_2	V_3	V_4	V_5
1.25	1.71 Vo	2.48 Vo	4.95 Vo	1.15 Vo	6.58 Vo
1.5	1.71 Vo	1.50 Vo	3.00 Vo	1.15 Vo	4.00 Vo
2.0	1.71 Vo	1.00 Vo	2.00 Vo	1.15 Vo	2.67 Vo
2.5	1.71 Vo	0.83 Vo	1.67 Vo	1.15 Vo	2.21 Vo

INEL-S-2032

Figure 13. Cross Section of a Horizontal Heat Exchanger Showing Velocity Variation Due to Shell and Tube Geometry ($V_3 = V_c$)

fraction of the distance between tubes. Also, the velocity between tubes becomes large.

Another problem created by cross-flow in horizontal vessels is the area of very low velocity directly above a tube. In model units, streaming past the tubes creates a pile of particles resting on top of the tubes. These areas are dead as far as heat transfer is concerned, and are potential locations for corrosive attack. Two possible methods of eliminating this problem are to induce internal circulation by means of baffles or to use spiral fluted tubing. Tests of these techniques have not been performed.

4. Proportioning Tubes - Disengagement Space

One technique for providing more uniform flow velocities in horizontal exchangers is to vary the pitch-to-tube diameter ratio proportional to the cross sectional area. At the bottom of the vessel the tubes would be spread about 33% further apart to produce the same velocity as seen at the midpoint cross section.

Disengagement space above the top of the bed must be designed into the heat exchanger. In liquid-fluidized-bed heat exchangers with particulate fluidization, the interface is definite and constant, but a small fraction of particles will have sufficient velocity to escape the top of the bed, and sufficient head room must be allowed for them to decelerate and drop back to the bed. Two to three inches is sufficient in a vertical vessel if the distribution is uniform. However, as a safety factor 5 to 6 inches is usually allowed. In horizontal vessels the current convention is to allow 25% of the vessel diameter at the top for disengagement. This is due to increasing fluid velocity in the top of the vessel. With larger vessels it may prove practical to allow less head space because there is a normal drop in velocity above the top row of tubes.

IV. Sample Design Problem

The design process for a liquid-fluidized-bed heat exchanger is similar to designing a conventional tube-and-shell exchanger. Several parameters which are not included in shell-and-tube units must be included:

1. The number of stages.
2. Shell-side velocity and consequently the shell cross-sectional area.
3. Particle size.
4. Flow distribution.
5. Disengagement space.

Present information indicates that a shell-side fouling factor is not required.

Parameters which are fixed include:

1. Brine inlet temperature.
2. Coolant inlet temperature.
3. Materials of construction.

Parameters which are varied to minimize system cost include:

1. Brine outlet temperature and brine mass flow rate.
2. Coolant outlet temperature and coolant mass flow rate.
3. Coolant tube-side velocity and the number of tubes.
4. Tube diameter.
5. Number of tube passes.

The design example considers a small liquid-liquid heat exchanger that would be used as a preheater in a small power system or in a non-electric application. For the example given, which corresponds to a small pre-heater for a binary electric plant, isobutane was used as the secondary fluid.

From the mass flow rate and required liquid isobutane velocity the number of tubes are calculated. For this case thirty-five 0.95-cm (3/8 inch), 18BWG tubes are required.

Table III

Conditions for Design of a
Liquid-Fluidized-Bed Preheater

Shell Material: Carbon Steel
Tube Material: 0.95 cm (3/8 inch) O.D. 316 Stainless Steel
Tube Wall Thickness: .124 cm (0.049 inch)
Number of Stages: 6
Particle Size: 1 mm MPD
Mass Flow Rate of Isobutane: 5,900 kg/hr (13,000 lb/hr)
Mass Flow Rate of Geothermal Fluid: 6,360 kg/hr (14,000 lb/hr)
Velocity of Isobutane in Tube-Side: 2.44 m/sec (8 ft/sec)
Velocity of Geothermal in Shell-Side: .051 m/sec (10 ft/min)
Temp. of Geothermal Fluid at Entrance: 107°C (225°F)
Temp. of Geothermal Fluid at Exit: 60°C (140°F)
Temp. of Isobutane at Entrance: 27°C (80°F)
Temp. of Isobutane at Exit: 99°C (210°F)

The first step in calculating the heat transfer surface area is to determine the log mean temperature difference (LMDT) for each stage. This is done from a plot similar to the one in Figure 14 where the quantities of heat for brine and isobutane are plotted against temperature. In this plot, the heat load is divided between stages to keep stage size reasonably uniform. The stair-step effect on the brine cooling curve results from the isothermal behavior of each fluidized-bed stage. The horizontal step represents the idealized mean bed temperature.

Inside film coefficients are estimated using the Seider-Tate correlation as shown in equation (18).[19]

$$h_i = \frac{0.27\,(C_{pb})(G)}{(R_{eb})^{0.2}\,(Nu)^{2.3}\,\left(\frac{\mu_{fw}}{\mu_f}\right)} \qquad (18)$$

The outside coefficient is either calculated from the correlation found in equation (17) or from a plot of data such as found in Figure 11. The overall heat transfer coefficient U is then calculated using equation (19).

$$\frac{1}{U} = \frac{1}{h_o} + \left(\frac{D_t}{k_m}\right) \ln\left(\frac{D_t}{D_i}\right) + \frac{1}{h_i}\left(\frac{D_t}{D_i}\right) + \frac{1}{f_i}\left(\frac{D_t}{D_i}\right) + \frac{1}{f_o} \qquad (19)$$

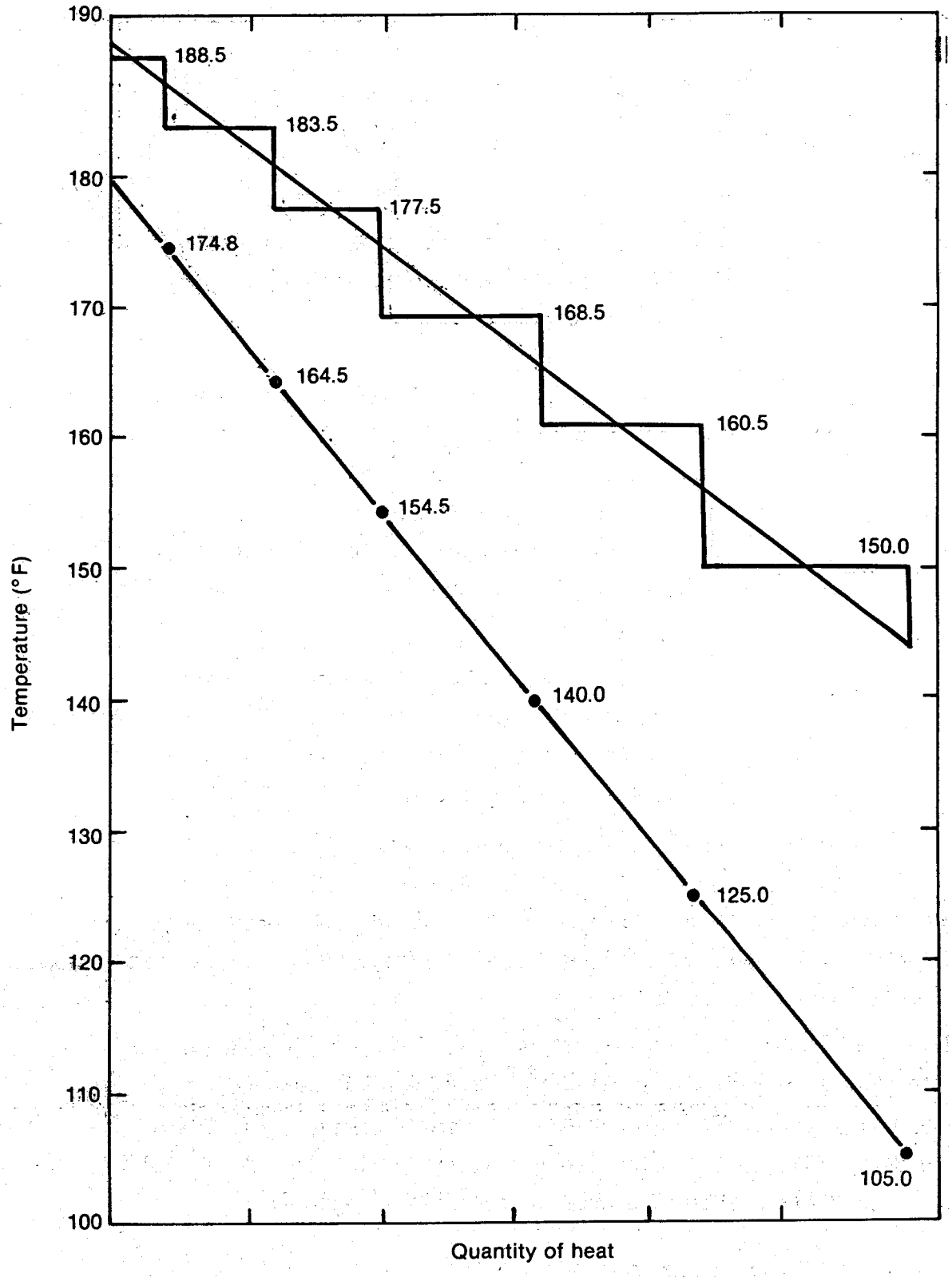

Figure 14. Division of Preheater into Six Stages; In This Case Division is Made to Produce Similar Size Stages

In laboratory bench-scale experiments, the outside tube fouling resistance ($\frac{1}{f_o}$) was found to be less than 5 x 10^{-6} M^2kW with a coil exchanger in synthetic brine. Normally this term is ignored. Inside fouling resistance for isobutane may be taken as 8.8 x 10^{-5} M^2k/W.

Using the value of the overall heat transfer coefficient (U) the heat transfer area (A) is calculated using equation (20).

$$A = \frac{Q}{U\ (LMTD)} \tag{20}$$

From the total required area, tube diameter, and number of tubes, the length of the tube bundle is calculated. From the number of tubes and tube pitch, the diameter of the shell is calculated. The geothermal velocity is then calculated and compared to the value used in determining the bed-to-tube heat transfer coefficient (h_o). If the velocities vary, several options are available as shown in Table IV.

Care must be exercised in reiterating to velocities which are too high or too low. The assumed value of velocity is normally chosen because it is close to the heat transfer maximum. The preferred method is to choose one of the other techniques for closing the gap between the assumed and calculated velocity, and then reiterate to fine tune.

For the 60 kW(e) pilot plant, three vertical stages and three horizontal stages were chosen; the calculated parameters are shown in Table IV. For demonstration only, three vertical stages and three horizontal stages were chosen to achieve the six stages. Normally, all stages would be of the same type.

When compared to conventional tube-and-shell exchangers designed for the same service, liquid-fluidized-bed heat exchangers require substantially less heat transfer surface. However, because of the higher pitch-to-tube diameter ratio, the shells tend to be larger, and consequently represent a greater fraction of the cost.

Table IV

Optional Ways of Matching Assumed to Calculated Shell-Side Velocities

	Horizontal Case	Vertical Case
Calc. velocity greater than assumed velocity	1. reiterate (avoid exceeding terminal vel.) 2. try larger particle size 3. increase P/dt diameter	1. reiterate (avoid exceeding terminal velocity) 2. try larger particle size 3. multipass secondary fluid 4. increase P/dt diameter
Calc. velocity less than assumed velocity	1. reiterate (avoid being less than fluidizing velocity) 2. try smaller particle size 3. decrease P/dt (may not be pos sible) 4. multipass secondary fluid	1. reiterate (avoid being less than fluidizing velocity) 2. try smaller particle size 3. decrease P/dt (may not be pos-sible)

Table V

Six-Stage, Six-Pass Liquid-Fluidized-Bed Preheater for a 60 $kW_{(e)}$ Geothermal Power Plant

	Stage No. 1	Stage No. 2	Stage No. 3	Stage No. 4	Stage No. 5	Stage No. 6
Temp. of liquid isobutane at entrance (^{o}C)	92	82	70	58	43	27
Temp. of liquid isobutane at exit (^{o}C)	99	92	82	70	58	43
Isothermal temp. of geothermal fluid (^{o}C)	105	99	92	84	76	66
Quantity of heat exchanged (W)	3.48×10^4	4.68×10^4	5.83×10^4	5.83×10^4	6.96×10^4	8.04×10^4
LMTD (^{o}C)	9.20	11.7	15.5	20.0	24.3	29.8
h_o geothermal fluid film coefficient (W/m^2k)	6640	6691	6640	6640	6640	6640
h_i liquid isobutane film coefficient (W/m^2k)	4142	4319	4194	4068	3978	3257
U overall heat transfer coefficient (W/m^2k)	1782	1827	1793	1765	1742	1702
Heat transfer area (m^2)	2.11	2.20	2.09	1.65	1.65	1.59
Effective tube length (m)	2.01	2.10	1.99	1.57	1.57	1.51
Tube length per pass (m)	.335	.349	.333	.338	.262	.251
Shell inside diameter (m)	.254	.254	.254	.254	.254	.254

References

1. Hogg, G.W. and Grimmett, E.S. "Effects of Pulsation on Heat Transfer in a Liquid Fluidized Bed", Chem. Eng. Prog. Symposium Series, 62 (67), 1966.

2. Botterill, S. S. M., Fluid Bed Heat Transfer, Academic Press, 1975.

3. Patel, R. D. and Simpson, J. M., Chem Eng. Sci., 32, 76, 1977.

4. Trupp, A. C., "A Review of Fluidization Relevant to a Liquid Fluidized Bed Nuclear Reactor", Witheshell Nuclear Establishment, Pinawa, Manitoba, Oct. 1967.

5. Wagner, K. L., Preliminary Study of Amorphous Silica Deposition in a Bench Scale Liquid Fluidized Bed Heat Exchanger, presented to the Scale Management in Geothermal Energy Development Conference, 1976.

6. Grimmett, E. S. "A Method of Determining Volumes and Surface Areas for Groups of Non-Uniform Sized Particles. AEC Research and Development Report IDO-14617, 1963.

7. Lewis, E.W. and Bowerman, E. W. "Fluidization of Solid Particles in Liquid", Chem. Eng. Progr. 49, 12, 1952, pp 603.

8. Richardson, J. F. and Zaki, W. N., Trans. Inst. Chem. Engrs., 32, 35, 1954.

9. Wilhelm, R. H. , Mooson Kwauk, "Fluidization of Solid Particles", C.P.E., Vol. 44, No. 3, 1948, pp 201.

10. Hamilton, William, "A Correlation for Heat Transfer in Liquid Fluidized Beds", Can. J. Chem. Engng., Vol. 48, 1970, pp 52.

11. Brea, F. M., W. Hamilton, "Heat Transfer in Liquid Fluidized Beds with a Concentric Heater", Trans. Instn. Chem. Engrs., Vol. 49, 1971, pp 196.

12. Richardson, J. E., M.N. Romani, K. J. Shakiri, "Heat Transfer from Immersed Surfaces in Liqui Fluidized Bed", Chem. Engng. Sci., Vol. 31, 1976, pp 614.

13. Ruckenstein, E., I. Teoreanu, "On Heat or Mass Transfer Between the Fluidizing Agent and the Solid Particles of Fluidized Beds", NP-tr-538, U.K.A.E.A., 1960.

14. Chu, J. C., James Kalil, William A. Wetteroth, "Mass Transfer in a Fluidized Bed", C.P.E., Vol. 49, No. 3, 1953, pp 141.

15. Wasmund, B., J. W. Smith, "Wall to Fluid Heat Transfer in Liquid Fluidized Beds", Can. J. Chem. Engng., Vol. 45, 1967, pp156.

16. Jagannadjaraju G. J. V. and Rao C. V., Indian J. Technol. 3, 201, 1965.

17. Allen, C. A., Fukuda, O., Grimmett, E. S. and McAtee, R. E. , "Liquid Fluidized Bed Heat Exchanger - Horizontal Configuration Experiments and Data Correlations", 12th Intersociety Energy Conversion Engineering Conference, Preprint, 1977.

18. Grimmett, E. S., Fanous, A. F., and Allen, C. A., "Advances in Liquid Fluidized Bed Heat Exchanger Developemtn", 1977 Heat Tranfer Conference, ASME 1977.

19. Sieder, E. N., and Tate, C. E., "Heat Transfer and Pressure Drop of Liquids in Tubes", Ind. Eng. Chem. 28, 142, 1936.

Nomenclature

A = heat transfer surface area
A_c = cross sectional area of the vessel
C = constant
C_{pb} = bulk heat capacity
D_c = drag coefficient (dimensionless)
D_s = diameter of shell
D_i = inside tube diameter
D_t = outside tube diameter
d_p = diameter of bed particle
F_k = kinetic force
f_i = inside fouling factor
f_o = outside fouling factor
g_c = gravitational constant
G = Sieder-Tate correlation coefficient
h_o = bed-to-tube heat transfer coefficient
h_i = inside tube heat transfer coefficient
J = Colburn J factor = $Nu/Re_o\ Pr^{1/3}$
J' = Chu's J Factor = $C(Re_o/1-\varepsilon)n-1$
k = thermal conductivity
LMTD = log mean temperature difference
m = exponent of equation (1.4)
M = mass of fluid
n = (n-1) is slope derived by Figure 7
Nu = hL/k Nusselt Number
P = tube pitch
Pr = $Cp\ \mu_s/h_f$
Re_b = bulk Reynolds number
Re_o = Reynolds number at superficial velocity $\rho_f\ Vo\ dp/\mu_f$
Re_t = Reynolds number at terminal velocity $\rho_f\ Vt\ dp/\mu_f$
U = overall heat transfer coefficient
u = tub-side velocity
v_c = velocity at the horizontal diameter of a horizontal heat exchanger
v_i = velocity at voidage of unity
v_o = superficial velocity
v_t = terminal velocity
v_{mf} = incipient velocity
ε = void fraction (porosity)
μ_f = viscosity of fluid
μ_w = viscosity of fluid at the wall
ρ_s = density of solid
ρ_f = density of fluid
Δp = pressure drop

DISTRIBUTION RECORD FOR ICP-1153

Internal Distribution

1 - Chicago Patent Group
9800 South Cass
Argonne, IL 60439

1 - R. L. Blackledge
Idaho Operations Office - DOE
Idaho Falls, ID 83401

1 - H. P. Pearson
Information Management, EG&G

10 - INEL Technical Library

45 - Author

External Distribution

531 - Distribution under UC-66d - GE: Utilization Technology

45 - Special External

Total Copies Printed: 634